The effect of scattering in surface wave tomography

Jesper Spetzler,* Jeannot Trampert and Roel Snieder[†]

Department of Geophysics, Utrecht University, PO Box 80.021, NL-3508 *TA Utrecht, The Netherlands. E-mail: j.spetzler@citg.tudelft.nl*

SUMMARY

We present a new technique in surface wave tomography that takes the finite frequency of surface waves into account using first-order scattering theory in a SNREI Earth. Physically, propagating surface waves with a finite frequency are diffracted by heterogeneity distributed on a sphere and then interfere at the receiver position. Paradoxically, surface waves have the largest sensitivity to velocity anomalies off the path of the geometrical ray. The non-ray geometrical effect is increasingly important for increasing period and distance. Therefore, it is expected that the violation of ray theory in surface wave tomography is most significant for the longest periods.

We applied scattering theory to phaseshift measurements of Love waves between periods of 40 and 150 s to obtain global phase velocity maps expanded in spherical harmonics to angular degree and order 40. These models obtained with scattering theory were compared with those constructed with ray theory. We observed that ray theory and scattering theory predict the same structure in the phase velocity maps to degree and order 25–30 for Love waves at 40 s and to degree and order 12–15 for Love waves at 150 s. For reasons of spectral leakage, a smoothness condition was included in the phaseshift inversions to construct the phase velocity maps, so we could not access the small length-scale structure in the obtained Earth models.

We carried out a synthetic experiment for phase velocity measurements to investigate the limits of classical ray theory in surface wave tomography. In the synthetic experiment, we computed, using the source–receiver paths of our surface wave data set, the discrepancy between ray theoretical and scattering theoretical phase velocity measurements for an input model with slowness heterogeneity for increasing angular degree. We found that classical ray theory in global surface wave tomography is only applicable for structures with angular degrees smaller than 25 (equivalent to 1600 km) and 15 (equivalent to 2700 km) for Love waves at 40 and 150 s, respectively. The synthetic experiment suggests that the ray theoretical great circle approximation is appropriate to use in present-day global surface wave tomography. On the other hand, in order to obtain reliable models with a higher resolution we must take the non-ray geometrical effect of surface waves into account.

Key words: finite-frequency effects, Fresnel zone, group velocity, phase velocity maps, ray theory, Rytov approximation, single-mode scattering theory.

1 INTRODUCTION

In surface wave tomography, global as well as regional models are being obtained with increasing resolution. This increase in spatial resolution allows a comparison between tomographic models and detailed tectonic features. Most techniques for surface wave tomography are based on simplified versions of ray theory; see, for instance, Backus (1964), Dziewonski (1984), Woodhouse &

Dziewonski (1984), Trampert & Woodhouse (1995), van der Lee & Nolet (1997) and van Heijst & Woodhouse (1999) who all apply the great circle approximation to compute Earth models from surface wave data. However, ray theory introduces an inconsistency from a methodological point of view. It is only valid if the length-scale of velocity perturbations is larger than the wavelength and the width of the Fresnel zone. This condition is often violated for high-resolution *S*-velocity models compiled with ray theory because the characteristic length of heterogeneity in present surface wave models is comparable with the width of Fresnel zones (Passier & Snieder 1995).

Several examples of scattering theory used to explain wave propagation in heterogeneous media are given in the literature. Yomogida

*Now at: Department of Applied Earth Sciences, Delft TU, PO Box 5028, NL-2600 GA Delft, The Netherlands. E-mail: j.spetzler@citg.tudelft.nl
[†]Now at: Department of Geophysics, Colorado School of Mines, Golden, CO 80401, USA.

& Aki (1987), Yomogida (1992), Woodward (1992), Snieder & Lomax (1996) and Spetzler & Snieder (2001) use the Rytov approximation to derive the frequency-dependent time-shift. In Spetzler & Snieder (2001), it is demonstrated explicitly that the time-shift can be computed as an integration of the slowness perturbation field multiplied by a sensitivity kernel (also known as the Fréchet kernel). Furthermore, Spetzler & Snieder (2001) confirm through a numerical experiment that the regime of scattering theory is important when the length-scale of inhomogeneity is smaller than the width of the Fresnel zone. Woodhouse & Girnuis (1982) and Snieder (1993) use normal-mode theory to compute the Fréchet kernel for degree l and order m in surface wave tomography using spherical harmonics to expand the slowness perturbation field. Marquering *et al.* (1998, 1999), Tong *et al.* (1998), Dahlen *et al.* (2000), Hung *et al.* (2000) and Zhao *et al.* (2000) apply a cross-correlation function to introduce the frequency-dependent time-shift in body wave tomography. It is shown in several of these articles that the sensitivity kernel for 3-D wave propagation vanishes on the geometrical ray and that the maximum sensitivity to slowness perturbations is off the path of the ray. However, surface wave tomography is a 2-D problem and the scattering theoretical sensitivity to slowness perturbations is non-zero on the ray path, although not maximum.

In this study, we develop a frequency-dependent scattering theory for minor and major arc surface waves by using the first-order Rytov approximation. The theory is applicable for unconverted surface waves in a SNREI Earth model. The scattering theory can be applied to both phase and group velocity measurements. Given the same strength of inhomogeneity, diffraction of surface waves becomes increasingly important when the dominant period in the phaseshift data set or the source–receiver distance increases. It is shown how relative phaseshifts and group delays measured from surface waves are related linearly to the coefficients of the spherical harmonics for relative phase and group velocity, respectively. Relative phaseshift measurements for Love waves at 40 and 150 s from Trampert & Woodhouse (2001) are inverted to obtain phase velocity maps using scattering theory.

We show a synthetic experiment wherein, given the source–receiver paths in our surface wave data set, the relative error introduced by ray theory is computed for slowness heterogeneities with increasing angular degree. The synthetic experiment shows that the diffraction of surface waves is dominant if the structure of the Earth exceeds an angular degree of 15 (corresponding to a length-scale of inhomogeneity of about 2700 km) for surface waves at 150 s and angular degree 25 (the characteristic length of heterogeneity is 1600 km) for surface waves at 40 s. This is close to the current limit of resolution that we obtain in the phase velocity maps in this work. In addition, the synthetic experiment demonstrates that small-scale structures in surface wave tomographic models obtained using ray theory may contain systematic errors.

In Section 2, the width of the Fresnel zone for surface waves is derived, and it is shown how to relate surface wave measurements (i.e. relative phaseshift and group delay) with relative phase and group velocity perturbations on a sphere using ray theory and scattering theory. Additionally, the properties of the Fréchet kernels owing to non-ray geometrical effects are discussed. In Section 3, the set-up of the surface wave experiment using Love waves between periods of 40 and 150 s is explained. In Section 4, the results of the inversion of relative phaseshifts for Love and Rayleigh waves at 40 and 150 s are given. In Section 5, a discussion of the small-scale structures of the Earth is given, and thereby the synthetic experiment is shown. The conclusions are drawn in Section 6.

2 THEORY

2.1 The width of Fresnel zones on the sphere

Fresnel zones are defined in terms of the difference in propagation length of rays with adjacent paths. The points inside the Fresnel zone are those points giving single-scattered waves that have a detour smaller than a certain fraction of the wavelength λ compared with the ballistic ray (e.g. Kravtsov 1988). This fraction of the wavelength is denoted by λ/n, where $n = 8/3$ for waves propagating in two dimensions (Spetzler & Snieder 2001). Physically, waves scattered by points inside the first Fresnel zone interfere constructively at the receiver position. In the rest of this paper, the Fresnel zone refers strictly speaking to the first Fresnel zone. It is shown in Appendix A how to derive the maximum width of Fresnel zones on the sphere. The epicentral distance between a given source and receiver geometry is denoted by Δ_{off}. The maximum width L_{F} of Fresnel zones in radians is then given by

$$L_{\text{F}} = \sqrt{\frac{3\lambda}{2} \tan\left(\frac{\Delta_{\text{off}}}{2}\right)}, \tag{1}$$

where $\Delta_{\text{off}} \in [0, \pi]$ and the wavelength is in radians. The width of Fresnel zones increases with increasing wavelength and epicentral distance. In the limit where the source–receiver distance goes towards π, the Fresnel zone converges to the whole sphere. The formula in eq. (1) is derived using second-order perturbation theory. Accordingly, the tangent function goes to infinity for the source–receiver offset Δ_{off} going to π (i.e. the approximation breaks down).

2.2 Phase and group velocity maps using ray theory

Trampert & Woodhouse (1995), for instance, apply the ray theoretical great circle approximation (e.g. Backus 1964; Jordan 1978; Dahlen 1979) to express the average relative phaseshift $\delta\varphi/\varphi_0$ along minor arcs (i.e. $0 < \Delta_{\text{off}} < \pi$) and major arcs (i.e. $\pi < \Delta_{\text{off}} < 2\pi$) in terms of the local relative phase velocity perturbation $\delta v/v_0$ averaged over the ray path between the source and receiver, hence

$$\frac{\delta\varphi}{\varphi_0}(\Delta_{\text{off}}) = -\frac{1}{\Delta_{\text{off}}} \int_{\mathbf{r}_S}^{\mathbf{r}_R} \frac{\delta v}{v_0}(\theta, \varphi) \, dr, \tag{2}$$

where dr is in radians. The location of the source and receiver on the unit sphere are denoted by S and R, respectively, and the epicentral distance between the source and receiver is Δ_{off}. Furthermore, Trampert & Woodhouse (1995) expand the local relative phase velocity perturbation as a sum over spherical harmonics, thus

$$\frac{\delta v}{v_0}(\theta, \varphi) = \sum_{l=0}^{l_{\text{max}}} \sum_{m=-l}^{l} C_l^m Y_l^m(\theta, \varphi). \tag{3}$$

The upper limit in the spherical expansion of the relative velocity perturbation is denoted by l_{max}, and the coefficient of spherical harmonics to angular degree l and order m for the relative phase velocity is written as C_l^m. The relative phaseshift is then expressed in spherical harmonics by inserting eq. (3) in eq. (2) which gives that

$$\frac{\delta\varphi}{\varphi_0}(\Delta_{\text{off}}) = \sum_{l=0}^{l_{\text{max}}} \sum_{m=-l}^{m=l} C_l^m K_{l,m}^{\text{ray,ph}}(\Delta_{\text{off}}), \tag{4}$$

with the ray theoretical sensitivity kernel for angular degree l and order m equal to

$$K_{l,m}^{\text{ray,ph}}(\Delta_{\text{off}}) = -\frac{1}{\Delta_{\text{off}}} \int_{\mathbf{r}_S}^{\mathbf{r}_R} Y_l^m(\theta, \varphi)\, dr. \tag{5}$$

Similarly, group velocity maps may be retrieved from group delays measured by bandpass-filtered surface waveforms. In terms of ray theory, the time-shift $\delta t(\Delta_{\text{off}})$ at epicentral distance Δ_{off} is given by

$$\delta t(\Delta_{\text{off}}) = \sum_{l=0}^{l_{\max}} \sum_{m=-l}^{m=l} U_l^m K_{l,m}^{\text{ray,gr}}(\Delta_{\text{off}}), \tag{6}$$

where the coefficient of spherical harmonics to degree l and order m for the relative group velocity is denoted by U_l^m, and the sensitivity kernel for relative group velocity is

$$K_{l,m}^{\text{ray,gr}}(\Delta_{\text{off}}) = -\frac{R}{u_0} \int_{\mathbf{r}_S}^{\mathbf{r}_R} Y_l^m(\theta, \varphi)\, dr. \tag{7}$$

The reference group velocity at the central frequency is denoted by u_0, and R is the radius of the Earth.

Ray theory is valid when the characteristic length a of heterogeneity is much larger than the wavelength λ and the width of Fresnel zones L_{F}. Hence in non-dimensional numbers the condition for ray theory is written as

$$\frac{\lambda}{a} \ll 1 \quad \text{and} \quad \frac{L_{\text{F}}}{a} \ll 1, \tag{8}$$

see Menke & Abbot (1990).

2.3 Phase and group velocity maps using scattering theory

The theory of diffracted surface waves is developed for minor and major arc measurements using the first-order Rytov approximation. First, the relative phaseshift for minor arcs is derived for a reference system using co-latitude coordinates with the source position at $(\pi/2, 0)$ and the receiver position at $(\pi/2, \Delta_{\text{off}})$. We derive the scattering sensitivity kernels, which linearly relate the relative phaseshift and group delay to the phase and group velocity, expanded in spherical harmonics. Then, we show how the kernels for major arcs using scattering theory are derived from the theory developed for minor arcs. Finally, we show that phase and group velocity measurements for any source–receiver configuration can be computed in a fast way using rotating tabulated sensitivity kernels in the reference system.

Snieder & Nolet (1987) and Snieder & Romanowicz (1988) linearize the Lamé coefficients λ and μ and the density ρ to write the Born vector wavefield $\mathbf{u}_1(\mathbf{r}_r)$ as

$$\mathbf{u}_1(\mathbf{r}_r) = \mathbf{P}(R, \theta_r, \varphi_r)[\mathbf{P}(R, \theta_s, \varphi_s) \cdot \mathbf{F}]$$
$$\times \int_0^{\Delta_{\text{off}}} \int_0^{\pi} \frac{\exp i \left(kR\Delta_2 + \pi/4\right)}{\sqrt{\frac{\pi}{2} kR \sin(\Delta_2)}}$$
$$\times V(R, \theta, \varphi) \frac{\exp i \left(kR\Delta_1 + \frac{\pi}{4}\right)}{\sqrt{\frac{\pi}{2} kR \sin(\Delta_1)}} R^2 \sin(\theta)\, d\theta\, d\varphi, \tag{9}$$

which is derived for wave propagation on the sphere. The adiabatic assumption (i.e. there is no mode conversion between different modes of Love and Rayleigh waves) is applied in eq. (9) so there is no summation over modes and mode conversions are absent. The polarization vector at the source (R, θ_s, φ_s) and at the receiver (R, θ_r, φ_r) is $\mathbf{P}$, the wavenumber is k for surface waves, the epicentral distances between the source and scatterer and between

the scatterer and receiver are denoted by Δ_1 and Δ_2, respectively, the Fourier transform of the point source function is $\mathbf{F}$ and the scattering coefficient is V. Snieder (1986) shows that for unconverted surface waves the interaction term V can be written as

$$V(R, \theta, \varphi) = -\frac{k^2}{2} \frac{\delta v}{v_0}(R, \theta, \varphi), \tag{10}$$

where the reference phase velocity and the phase velocity perturbation is v_0 and δv, respectively. The expression for the interaction term in eq. (10) is strictly speaking valid for forward scattering only. However, according to Snieder (1988), the surface wave radiation patterns for unconverted modes do not vary much as a function of the scattering angle, which implies that the scattering term in eq. (10) is a reasonable approximation for near-forward scattering at scatterer points inside the Fresnel zone.

Given the measurement of the i-component of the displacement, the average phaseshift $\delta\varphi^{(i)}(\Delta_{\text{off}}, \nu)$ along the path of the surface waves is obtained from

$$\delta\varphi^{(i)}(\Delta_{\text{off}}, \nu) = \text{Im}\left[\frac{u_1^i(\mathbf{r}_r)}{u_0^i(\mathbf{r}_r)}\right], \tag{11}$$

where the unperturbed vector wavefield $\mathbf{u}_0(\mathbf{r}_r)$ is given by

$$\mathbf{u}_0(\mathbf{r}_r) = \mathbf{P}(R, \theta_r, \varphi_r) \frac{\exp i \left(kR\Delta_{\text{off}} + \frac{\pi}{4}\right)}{\sqrt{\frac{\pi}{2} kR \sin(\Delta_{\text{off}})}} [\mathbf{P}(R, \theta_s, \varphi_s) \cdot \mathbf{F}], \tag{12}$$

for the epicentral distance Δ_{off} between the source and receiver (Snieder 1986). The expression in eq. (11) generalizes the Rytov approximation (e.g. Yomogida & Aki 1987; Snieder & Lomax 1996; Spetzler & Snieder 2001) to elastic waves.

The detour $\Delta_1 + \Delta_2 - \Delta_{\text{off}}$ and the geometrical factors $\sin(\Delta_1)$ and $\sin(\Delta_2)$ in eq. (9) are perturbed to second and zeroth order in the path deflection $(\theta - \frac{\pi}{2})$, respectively. For a source–receiver geometry along the equator line, the detour is given by

$$\Delta_1 + \Delta_2 - \Delta_{\text{off}} \approx \frac{\left(\theta - \frac{\pi}{2}\right)^2}{2} \frac{\sin(\Delta_{\text{off}})}{\sin(\varphi)\sin(\Delta_{\text{off}} - \varphi)}, \tag{13}$$

and the geometrical factors are

$$\sin(\Delta_1) \approx \sin(\varphi) \quad \text{and} \quad \sin(\Delta_2) \approx \sin(\Delta_{\text{off}} - \varphi), \tag{14}$$

(see Appendix A). The relative average phaseshift $\delta\varphi^{(i)}/\varphi_0(\Delta_{\text{off}}, \nu)$ at the single frequency ν is derived by inserting eqs (9), (10) and (12) in eq. (11), dividing by the phase $\varphi_0 = 2\pi \nu R \Delta_{\text{off}}/v_0$ and finally using the Taylor approximation for the detour and for the geometrical factors in eqs (13) and (14), respectively. Finally, the single-frequency relative phaseshifts $\delta\varphi^{(i)}/\varphi_0(\Delta_{\text{off}}, \nu)$ have to be integrated over a frequency band from $\nu_0 - \Delta\nu$ to $\nu_0 - \Delta\nu$, since phase velocity measurements at a single frequency are not possible owing to the finite sampling of the seismograms and the finite parametrization of the dispersion curve in the measurement process. Hence, the relative average phaseshift $\delta\varphi^{(i)}/\varphi_0(\Delta_{\text{off}}, \nu_0)$ at a central frequency ν_0, including non-ray geometrical effects, is given by

$$\frac{\delta\varphi^{(i)}}{\varphi_0}(\Delta_{\text{off}}, \nu_0) = \int_0^{\Delta_{\text{off}}} \int_0^{\pi} K^{\text{ph}}(R, \theta, \varphi) \frac{\delta v}{v_0}(R, \theta, \varphi)\, d\theta\, d\varphi. \tag{15}$$

The sensitivity kernel $K^{\text{ph}}(R, \theta, \varphi)$ for the relative phase velocity perturbation field is given by

$$K^{\mathrm{ph}}(R, \theta, \varphi) = -\frac{\sin(\theta)\sqrt{R\sin(\Delta_{\mathrm{off}})}}{2\Delta\nu\Delta_{\mathrm{off}}}$$

$$\times \int_{\nu_0-\Delta\nu}^{\nu_0+\Delta\nu} \frac{\sqrt{\nu}\sin\left[\frac{\pi\nu R}{\nu_0(\nu)}\left(\theta-\frac{\pi}{2}\right)^2 \frac{\sin(\Delta_{\mathrm{off}})}{\sin(\varphi)\sin(\Delta_{\mathrm{off}}-\varphi)} + \frac{\pi}{4}\right]}{\sqrt{\nu_0(\nu)\sin(\varphi)\sin(\Delta_{\mathrm{off}}-\varphi)}}\, d\nu,$$

$$(16)$$

where the reference velocity $\nu_0(\nu)$ generally depends on the frequency.

The relative velocity perturbation $\frac{\delta\nu}{\nu_0}(R, \theta, \varphi)$ is written as an expansion of spherical harmonics as shown in eq. (3). The relative phaseshift in eq. (15) is then given by

$$\frac{\delta\varphi^{(i)}}{\varphi_0}(\Delta_{\mathrm{off}}, \nu_0) = \sum_{l=0}^{l_{\max}} \sum_{m=-l}^{l} C_l^m$$

$$\times \int_0^{\Delta_{\mathrm{off}}} \int_0^{\pi} Y_l^m(\theta, \varphi) K^{\mathrm{ph}}(R, \theta, \varphi)\, d\theta\, d\varphi$$

$$= \sum_{l=0}^{l_{\max}} \sum_{m=-l}^{l} C_l^m K_{l,m}^{\mathrm{scat,ph}}(\Delta_{\mathrm{off}}, \nu_0). \qquad (17)$$

The right-hand side of the relative phaseshift caused by scattering in eq. (17) has the same form as the ray theoretical phaseshift in eq. (4), but with the scattering sensitivity kernel at the central frequency ν_0 for minor arcs given by

$$K_{l,m}^{\mathrm{scat,ph}}(\Delta_{\mathrm{off}}, \nu_0) = \int_0^{\Delta_{\mathrm{off}}} \int_0^{\pi} Y_l^m(\theta, \varphi) K^{\mathrm{ph}}(R, \theta, \varphi)\, d\theta\, d\varphi. \quad (18)$$

The sensitivity kernels needed to obtain group velocity maps using scattering theory can easily be derived from those for phase velocity. To see this, we start from the fundamental relation connecting group velocity u and phase velocity v,

$$u = \frac{v}{1 - \frac{v}{v}\frac{\partial v}{\partial v}}. \qquad (19)$$

Using first-order perturbation theory on eq. (19), the relative group velocity $\delta u/u$ expressed as $\delta(1/u)$ can be related to $\delta(1/v)$ (proportional to the relative phase velocity) through

$$\delta\frac{1}{u} = \delta\frac{1}{v} + 2\frac{\nu\delta v}{v^3}\frac{\partial v}{\partial v} - \frac{v}{v^2}\frac{\partial\delta v}{\partial v}, \qquad (20)$$

where the second term and third term take the dispersion of the reference phase velocity and phase velocity perturbation, respectively, into account. Differentiation of the relative phase velocity with respect to frequency leads to

$$\frac{\partial(\delta v/v)}{\partial v} = \frac{1}{v}\frac{\partial\delta v}{\partial v} - \frac{\delta v}{v^2}\frac{\partial v}{\partial v}. \qquad (21)$$

Eq. (21) is inserted in eq. (20), and we find that

$$\delta u/u = \delta v/v + v\frac{u}{v}\frac{\partial(\delta v/v)}{\partial v}. \qquad (22)$$

Noting that the relative phase velocity perturbation is minus the relative phaseshift and defining kernels similar to eq. (15), we may write that

$$K^{\mathrm{gr}}(R, \theta, \varphi) = -\frac{R\Delta_{\mathrm{off}}}{2\Delta\nu}\int_{\nu_0-\Delta\nu}^{\nu_0+\Delta\nu}\left[\frac{1}{u(\nu)}K^{\mathrm{ph}}(R, \theta, \varphi)\right.$$

$$\left. + \frac{v}{v(\nu)}\frac{\partial K^{\mathrm{ph}}(R, \theta, \varphi)}{\partial v}\right]d\nu, \qquad (23)$$

where here K^{ph} has to be taken at a single frequency rather than frequency averaged as in eq. (16). The measured group delay at a central frequency ν_0 can then be expressed as

$$\delta t^{(i)}(\Delta_{\mathrm{off}}, \nu_0) = \sum_{l=0}^{l_{\max}} \sum_{m=-l}^{l} U_l^m K_{l,m}^{\mathrm{scat,gr}}(\Delta_{\mathrm{off}}, \nu_0), \qquad (24)$$

where the minor arc, scattering theoretical sensitivity kernel for the relative group velocity in eq. (24) is given by

$$K_{l,m}^{\mathrm{scat,gr}}(\Delta_{\mathrm{off}}, \nu_0) = \int_0^{\Delta_{\mathrm{off}}} \int_0^{\pi} Y_l^m(\theta, \varphi) K^{\mathrm{gr}}(R, \theta, \varphi)\, d\theta\, d\varphi, \qquad (25)$$

The frequency averaging in eq. (23) has to correspond to the band-pass of the filter used in the group delay measurement.

The relative phaseshift for major arcs is obtained using the scattering theory for minor arcs. This is because major arc scattering sensitivity kernels can be constructed from three scattering sensitivity kernels for minor arcs; one sensitivity kernel for the minor arc between the source S and the receiver antipod RA, between the receiver antipod and the source antipod SA and between the source antipod and the receiver R, respectively. For major arcs, the scattering sensitivity kernel for relative phase velocity derived in the reference system is

$$K_{l,m}^{\mathrm{scat,ph}}(\Delta_{\mathrm{off}}, \nu_0) = \frac{1}{\Delta_{\mathrm{off}}}\left[(\Delta_{\mathrm{off}} - \pi)K_{l,m}^{\mathrm{scat,ph},S\to RA}(\Delta_{\mathrm{off}} - \pi, \nu_0)\right.$$

$$+ (2\pi - \Delta_{\mathrm{off}})K_{l,m}^{\mathrm{scat,ph},RA\to SA}(2\pi - \Delta_{\mathrm{off}}, \nu_0)$$

$$\left. + (\Delta_{\mathrm{off}} - \pi)K_{l,m}^{\mathrm{scat,ph},SA\to R}(\Delta_{\mathrm{off}} - \pi, \nu_0)\right], \qquad (26)$$

where $K_{l,m}^{\mathrm{scat,ph},S\to RA}(\Delta_{\mathrm{off}} - \pi, \nu_0)$, $K_{l,m}^{\mathrm{scat,ph},RA\to SA}(2\pi - \Delta_{\mathrm{off}}, \nu_0)$ and $K_{l,m}^{\mathrm{scat,ph},SA\to R}(\Delta_{\mathrm{off}} - \pi, \nu_0)$ are the relative phase velocity sensitivity kernels owing to scattering for the minor arc between the source and receiver antipod, between the receiver antipod and the source antipod and between the source antipod and receiver, respectively. Similarly, the major arc sensitivity kernel for the relative group velocity using scattering theory is given by

$$K_{l,m}^{\mathrm{scat,gr}}(\Delta_{\mathrm{off}}, \nu_0) = K_{l,m}^{\mathrm{scat,gr},S\to RA}(\Delta_{\mathrm{off}} - \pi)$$

$$+ K_{l,m}^{\mathrm{scat,gr},RA\to SA}(2\pi - \Delta_{\mathrm{off}}, \nu_0)$$

$$+ K_{l,m}^{\mathrm{scat,gr},SA\to R}(\Delta_{\mathrm{off}} - \pi, \nu_0). \qquad (27)$$

The expansions in eqs (26) and (27) are derived in Appendix B.

Dziewonski (1984) and Dahlen & Thromp (1998) explain how to rotate the reference system so that the source–receiver configuration, originally aligned along the equator, can be anywhere on the sphere. In Appendix C, the relative phaseshift related to the relative phase velocity for any minor arc, as well as major arc is derived. The sensitivity kernel in the observed coordinate system is given by

$$K_{l,m}^{\mathrm{scat,ph}}(\Delta_{\mathrm{off}}, \nu_0) = \exp(im\Phi)\sum_{n=-l}^{l}\exp(in\Psi)Q_l^{m,n}(\Theta)$$

$$\times K_{l,n}^{\mathrm{scat,ph}}(\Delta_{\mathrm{off}}, \nu_0), \qquad (28)$$

where Φ, Ψ and Θ are the three Euler angles, $Q_l^{m,n}(\Theta)$ are the elements of the rotation matrix and the sensitivity kernel $K_{l,n}^{\mathrm{scat,ph}}(\Delta_{\mathrm{off}}, \nu_0)$ is computed in the reference system where the source and receiver lie on the equator. This result also holds for group velocity measurements.
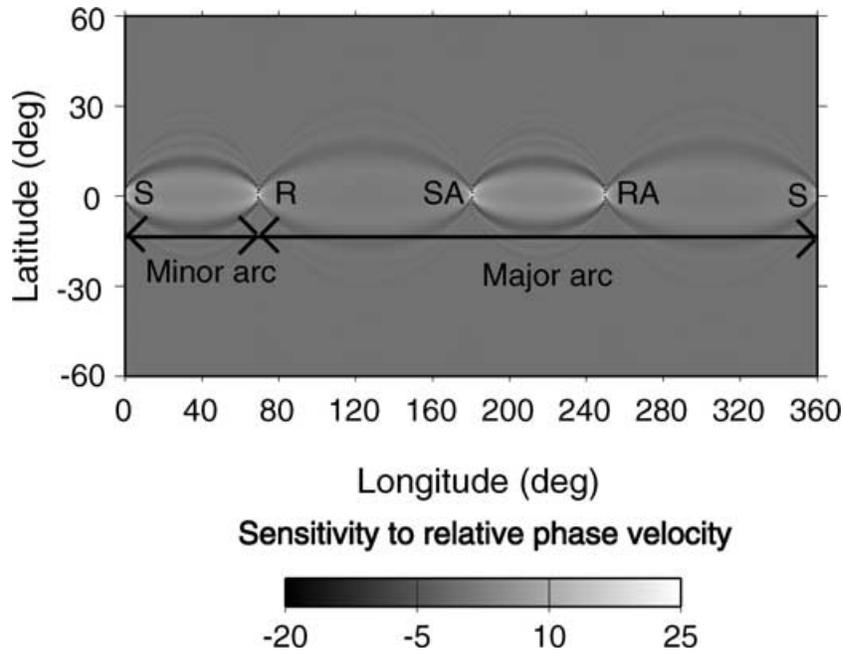
Figure 1. The scattering sensitivity kernel for relative phase velocity perturbations computed point by point on the sphere. The epicentral distance is 70° for the minor arc and 290° for the major arc. The central period of the sensitivity kernel is 150 s. The source position is denoted by *S*, the receiver antipode position by *R A*, the source antipode position by *S A* and the receiver position by *R*. The sensitivity kernel owing to scattering theory for the major arc surface wave is constructed by three scattering sensitivity kernels for minor arc surface waves. The first Fresnel zone is clearly visible, while sidelobes of the sensitivity kernel vanish owing to the frequency-averaging, inherent to the measurement. At this period, the relative phaseshift is therefore only sensitive to the relative phase velocity inside the Fresnel zone.

The regime of surface wave scattering theory is significant when the scalelength of heterogeneity is smaller than the width of the Fresnel zone (e.g. the conditions for ray theory are not satisfied). Let the characteristic length of the inhomogeneity be $a = 2\pi / l$ (in radians) for angular degree l. By using the condition for scattering theory, we can derive the limits of classical ray theory expressed in the angular degree of the spherical harmonics. Hence, when

$$\frac{L_F}{a} > 1 \Rightarrow l > \sqrt{\frac{8\pi^2}{3\lambda \tan(\Delta_{\text{off}}/2)}}, \tag{29}$$

the regime of scattering theory is important.

2.4 The properties of the scattering sensitivity kernels

Although we give explicit expressions for group velocity kernels, in the following, we are only discussing phase velocity kernels.

If the reference velocity is (approximately) constant, the frequency integration in the sensitivity kernel owing to scattering theory in eq. (16) can be performed analytically. The integration of the function $\sqrt{x} \sin(ax + \pi/4)$ is

$$\int \sqrt{x} \sin\left(ax + \frac{\pi}{4}\right) dx = \frac{\sqrt{x}}{\sqrt{2}a}\left[\sin(ax) - \cos(ax)\right] + \frac{\sqrt{\frac{\pi}{4}}}{a^{3/2}}$$
$$\times \left[C\left(\sqrt{\frac{2ax}{\pi}}\right) - S\left(\sqrt{\frac{2ax}{\pi}}\right)\right], \tag{30}$$

where the functions C and S are the Fresnel cosine and sine integrals, respectively. See Abramowitz & Stegun (1970) for a description of the Fresnel cosine and sine integrals. This analytical result can be used to compute the scattering sensitivity kernels in eqs (18) and

(25) in an efficient and accurate manner. On the other hand, if the reference velocity is dispersive, the frequency integration must be carried out numerically.

It is instructive to look at the sensitivity kernel for the relative local phase velocity for a minor arc surface wave and a major arc surface wave as shown in Fig. 1. The source position is located at a latitude (0°, 0°), and the receiver position is at (0°, 70°), thus the epicentral distance for the minor arc is 70°, while for the major arc the source–receiver distance is 290°. The radius of the sphere is set to 6371 km. The sensitivity to the relative phase velocity is computed with eq. (16) using the PREM phase velocity for Love waves as a reference velocity and the half frequency band $\Delta\nu = 2.5$ mHz for the phase velocity measurements of Trampert & Woodhouse (2001). The black zones in the near-field of the source, source antipod, receiver antipod and receiver show the singularities in the geometrical factors of the scattering sensitivity kernels for minor and major arcs. In form, the sensitivity kernel resembles the Fresnel zones for point sources. It clearly shows the first Fresnel zone, while higher-order Fresnel zones are less visible because of the frequency averaging, inherent to the measurement. Scattering sensitivity kernels for phase velocity measurements are also shown by Woodhouse & Girnius (1982) and Snieder (1993) who apply normal-mode theory to compute the sensitivity to slowness perturbations owing to scattering theory in surface wave tomography. Note that the sensitivity kernels in Woodhouse & Girnius (1982) and Snieder (1993) have oscillations along the great circle as a result of the interference of different surface wave orbits. In contrast, the ray-theoretical sensitivity kernel is only non-zero on the great circle passing through the source and receiver at 0° latitude.

In Fig. 2, cross-sections of scattering sensitivity kernels similar to that in Fig. 1 are plotted for different periods and epicentral offsets. The sensitivity kernels are shown at half the epicentral offset

(a) Epicentral distance = 160 degrees

(b) Period = 150 sec
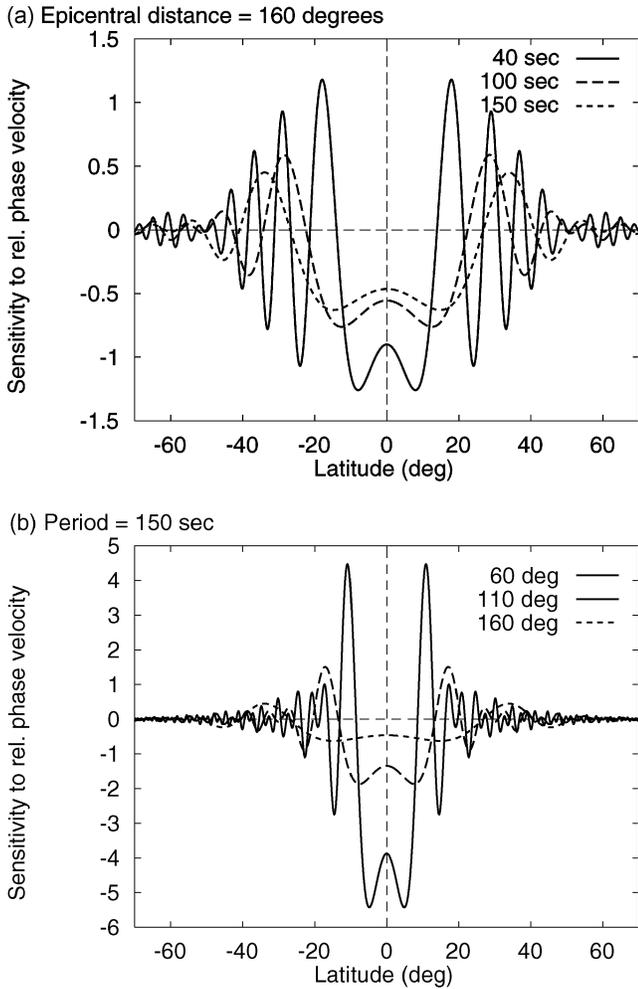
Figure 2. Cross-sections of the scattering sensitivity kernels for relative phase velocity perturbations computed at the half epicenal distance. (A) The epicentral distance is $160°$ for the three curves. The cross-section of the sensitivity kernel for relative phase velocity fluctuations is computed for the central period at 40 s (solid line), 100 s (dashed line) and 150 s (dotted line). (B) Sensitivity kernels at the central period of 150 s for relative phase velocity fluctuations. The epicentral distance for the cross-section of the scattering sensitivity kernel is $60°$ (solid line), $110°$ (dashed line) and $160°$ (dotted line).

where the width of the Fresnel zone is maximum. In Fig. 2(A), the sensitivity kernels for relative phase velocity are estimated for periods at 40 s (solid line), 100 s (dashed line) and 150 s (dotted line) using the PREM model for the reference velocity, the half frequency-band $\Delta \nu = 2.5$ mHz, and the epicentral distance is set to $160°$. For the short-period sensitivity kernel at 40 s, the sidelobes do not cancel out completely, whereas they have almost disappeared in the long-period Fréchet kernel at 150 s. We noticed that computing the scattering sensitivity kernel using the PREM phase velocity at the central frequency as a constant reference velocity in the whole frequency range yields virtually identical result to using the frequency-dependent PREM phase velocity in the range of frequency integration. The sensitivity kernels in Fig. 2(B) are computed with the period fixed to 150 s, and the epicentral distance is $60°$ (solid line), $110°$ (dashed line) and $160°$ (dotted line). The frequency band is again 2.5 mHz. In brief, Fig. 2 shows that the width of the central lobe of the scattering sensitivity kernel increases for increasing period and source–receiver distance.

Ray theory and scattering theory predict the same relative phaseshift when the length-scale of heterogeneity is larger than the width of the Fresnel zone (i.e. the condition for the regime of ray theory) since it follows from expression (16) that

$$\int_0^{\Delta_{\mathrm{off}}} \int_0^{\pi} K^{\mathrm{ph}}(R, \theta, \varphi) \frac{\delta v}{v_0}(R, \theta, \varphi) \, d\theta \, d\varphi$$
$$= -\frac{1}{\Delta_{\mathrm{off}}} \int_0^{\Delta_{\mathrm{off}}} \frac{\delta v}{v_0}(\theta, \varphi) \, dr, \tag{31}$$

when the characteristic length of the relative phase velocity is larger than the width of the Fresnel zone.

The maximum width W of the central lobe of the scattering sensitivity kernel is computed by setting the sine function in eq. (16) equal to zero, hence

$$0 = \sin\left[\frac{\pi \nu R}{v_0(\nu)} \left(\theta - \frac{\pi}{2}\right)^2 \frac{\sin(\Delta_{\mathrm{off}})}{\sin(\varphi)\sin(\Delta_{\mathrm{off}} - \varphi)} + \frac{\pi}{4} \right]$$
$$\Rightarrow \left(\theta - \frac{\pi}{2}\right)^2 = \frac{3\lambda}{4} \frac{\sin(\varphi)\sin(\Delta_{\mathrm{off}} - \varphi)}{\sin(\Delta_{\mathrm{off}})}, \tag{32}$$

where $\lambda = v_0(\nu)/(\nu R)$ is the central wavelength in radians. The maximum width $W = 2|\theta - \pi/2|$ of the central lobe is obtained by setting $\varphi = \Delta_{\mathrm{off}}/2$ in eq. (32) which gives

$$W = \sqrt{\frac{3\lambda}{2} \tan\left(\frac{\Delta_{\mathrm{off}}}{2}\right)}. \tag{33}$$

By comparing the maximum width of the central lobe in eq. (33) with the width L_{F} of Fresnel zones on the sphere in eq. (A8), the number n that defines the width of the Fresnel zone is given by

$$n = \frac{8}{3}. \tag{34}$$

This result is also derived in Spetzler & Snieder (2001) in a 2-D, Cartesian coordinate system. Additionally, we identify the central lobe of the scattering sensitivity kernel as the Fresnel zone on the sphere.

According to eq. (29), scattering theory is significant when the width of the Fresnel zone is larger than the length-scale of heterogeneity. We see in Fig. 2 that the Fresnel zone of surface waves enlarges for increasing period and epicentral offset. Therefore, given the same strength of heterogeneity, scattering theory is most important for the longest-period surface waves and if there are many long epicentral offsets in a given surface wave data set.

3 SETUP OF THE SURFACE WAVE EXPERIMENT

The data set of observed average relative phaseshifts is from Trampert & Woodhouse (2001), who calculate global phase velocity maps of Love and Rayleigh waves for periods between 40 and 150 s using the great circle approximation. We use these 41 000 phaseshifts to compute new phase velocity maps for Love waves at 40 and at 150 s, but using the fundamental-mode surface wave scattering theory.

The maximum degree of the spherical expansion of the phase velocity maps is 40, thus the number of unknown model parameters to be inverted is 1681. In addition, we use the same inversion procedure as Trampert & Woodhouse (2001); an *a priori* Laplacian smoothness condition is implemented so that truncation problems are avoided. In this manner, using the same data set and inversion

(a) Difference (scat-ray): Love 40 sec

Rel. phase velocity perturbations (%)

-2   0   2

(b) Difference (scat-ray): Love 150 sec

Rel. phase velocity perturbations (%)

-2   0   2
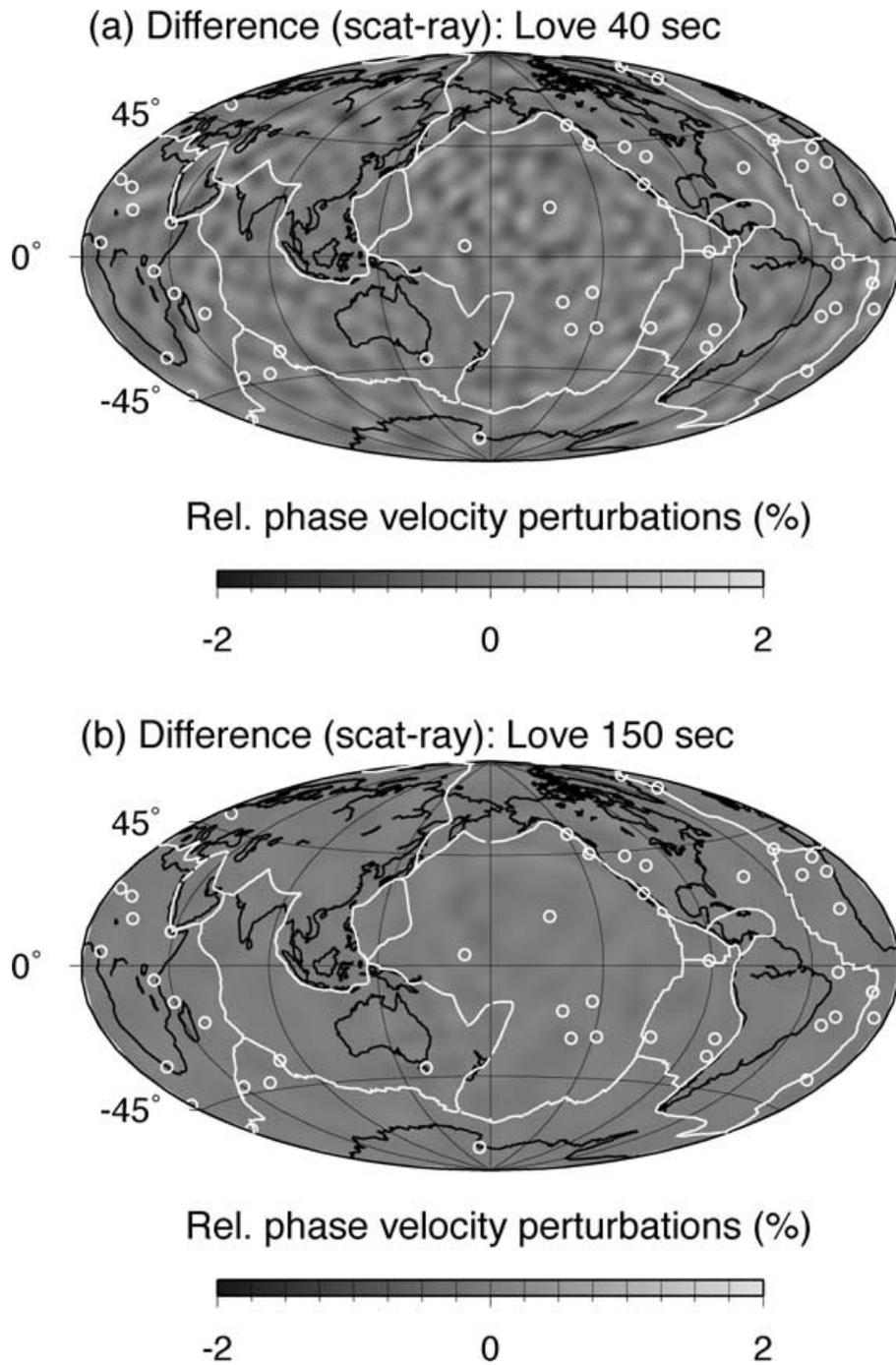
Figure 3. The difference between the phase velocity maps obtained using scattering theory and ray theory for Love wave at 40 and 150 s. The difference in relative phase velocity are given in per cent on a scale between ±2 per cent. Plate boundaries and hotspots are drawn with white lines and circles, respectively. The coastlines are marked with black lines on the difference between the phase velocity maps compiled using scattering theory and ray theory. (A) Love wave at 40 s. The smoothness factor $\gamma = 1 \times 10^{-4}$. (B) Love waves at 150 s. The smoothness factor $\gamma = 1 \times 10^{-2}$.

method, it is possible to make a direct comparison between global phase velocity maps between periods at 40 and 150 s inferred from ray theory and scattering theory, respectively.

4   RESULTS

In this section, we present the phase velocity maps from Love wave phase measurements between periods of 40 and 150 s that are ob-

tained with ray theory and scattering theory, respectively. We do not show any results for Rayleigh waves, which lead to the same conclusions. We hardly find any discrepancy between the phase velocity maps for Love waves at either 40 and 150 s obtained from ray theory and scattering theory. The difference between the phase velocity maps compiled with scattering theory and those computed using ray theory are shown in Figs 3(A) and (B) for the global Love wave experiment at 40 and 150 s, respectively.
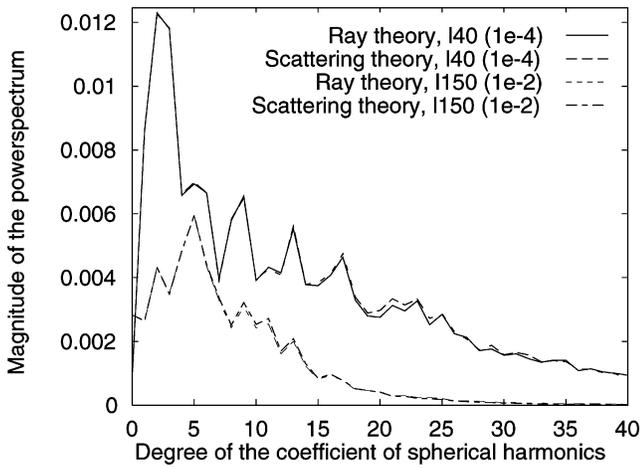
Figure 4. The power spectra of the estimated phase velocity maps for Love waves at 40 and 150 s using ray theory and scattering theory. The degree of the coefficients of spherical harmonics is shown on the abscissa, while the magnitude of the power spectra is plotted on the ordinate. It is observed that the phase velocity models for Love waves at 40 and 150 s have the same large-scale structure when using scattering theory and ray theory. However, it is not possible to obtain reliable smaller-scale structures in the obtained phase velocity maps because the observed relative phaseshifts require a Laplacian smoothing. The smoothness factors applied in the inversion of phase velocity measurements for Love waves at 40 and 150 s are the numbers given in parentheses.

The power spectra of the phase velocity maps in Fig. 4 confirm the qualitative observation that ray theory and scattering theory produce the same models. For Love waves at 40 s, the Laplacian smoothness factor $\gamma = 1 \times 10^{-4}$, while for the surface wave study at 150 s, $\gamma = 1 \times 10^{-2}$. Phase measurements for Love waves at 150 s are noisier, which would cause small-scale instabilities in the phase velocity maps using too small a value for the smoothness factor. Owing to the Laplacian smoothness parameter, small-scale structures for angular degrees higher than 20–25 and 10–15 (e.g. heterogeneity with a characteristic length of 1600–2000 and 2700–4000 km) are strongly suppressed in the phase velocity maps for Love waves at 40 and 150 s, respectively.

The smoothness parameters for the scattering theoretical inversion of Love waves at 40 and 150 s are determined in the following way; the derivative matrix **G** (see Menke 1989) built from the kernels $K_{l,m}$ is not the same for ray and scattering theory. Thus, the two theories will, in general, not resolve models identically for a given smoothness parameter. We require that for a given period the trace of the resolution matrix for ray theory is close to that for scattering theory. We then can compare models built from the same number of parameters.

5 DISCUSSION

In the inversion of Love wave phase shift data between periods of 40 and 150 s, ray theory and scattering theory retrieve the same large-scale structures as shown in Fig. 3. Because of the large value of the smoothness parameter, it is not possible to comment on the presence of smaller-scale structures in the Earth. In order to examine a possible discrepancy between ray theory and scattering theory in surface wave tomography, synthetic tests have to be carried out using an input model with heterogeneity much smaller in size than the width of the Fresnel zone.
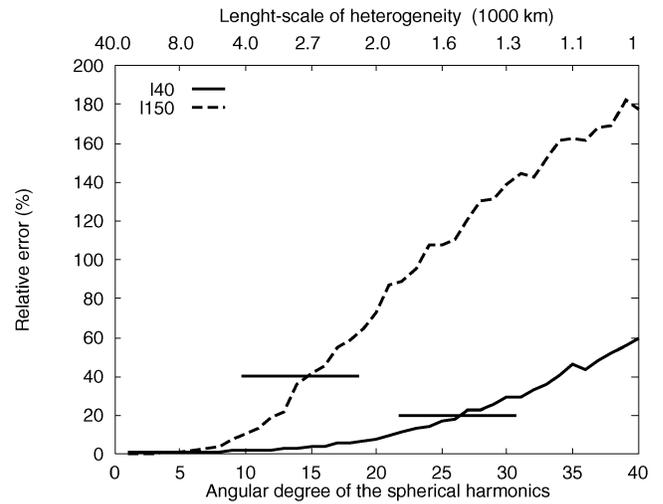
Figure 5. The synthetic experiment for phase velocity measurements showing that the relative error introduced by ray theory increases for decreasing characteristic length of velocity anomalies in a global surface wave experiment with Love waves between 40 and 150 s. The length-scale of heterogeneity is expressed in angular degree ranging between 1 and 40. The relative error between surface wave data owing to ray theory and scattering is calculated using the source–receiver positions in the Love wave data set. The thick horizontal line indicates the observed relative error at each period.

Spetzler & Snieder (2001) and Spetzler *et al.* (2002) show that scattering theory is very accurate in the prediction of time-shifts obtained from a finite-difference solution of the acoustic wave equation and from a laboratory ultrasonic wave experiment, respectively, wherein the length-scale of heterogeneity is smaller than the width of the Fresnel zone. We assume that the same holds for surface wave tomography, meaning that the discrepancy shown below is entirely the result of the inadequacy of ray theory.

In Fig. 5, we show with a synthetic surface wave experiment that the discrepancy between ray theory and diffraction theory in global surface wave tomography is important for heterogeneity with the angular degree larger than $l = 25$ and 15 for Love waves at 40 and 150 s, respectively. These estimations are slightly lower than those published in Spetzler *et al.* (2001) owing to a problem we found in our frequency averaging code. The fundamental conclusion, however, that our current models are close to the limits of validity of ray theory remains unchanged. We define the relative error (in per cent) introduced by ray theory using the source and receiver positions of our Love wave data set as

$$\text{relative error} = \frac{100 \text{ per cent}}{N} \sum_{i=1}^{N} \left| \frac{d_i^{\text{ray}} - d_i^{\text{scat}}}{d_i^{\text{scat}}} \right|, \quad (35)$$

where N is the number of source–receiver geometries and d_i^{ray} and d_i^{scat} are the surface wave data owing to ray theory and scattering theory, respectively. To avoid numerical instability, source–receiver pairs with $|d_i^{\text{scat}}| \leq 1 \times 10^{-3}$ for phase velocity measurements have not been included in eq. (35). The velocity perturbation is set to 10 per cent and the angular order m is fixed to zero, while the angular degree goes from 1 to 40, corresponding to a velocity heterogeneity of between 40 000 and 1000 km in the synthetic experiment. The ray theoretical approach based on the great circle approximation and the first-order scattering theory are both linear theories, so the amplitude of the velocity perturbation does not influence the relative error in eq. (35). Thus, for realistic Earth models with either a white or a red
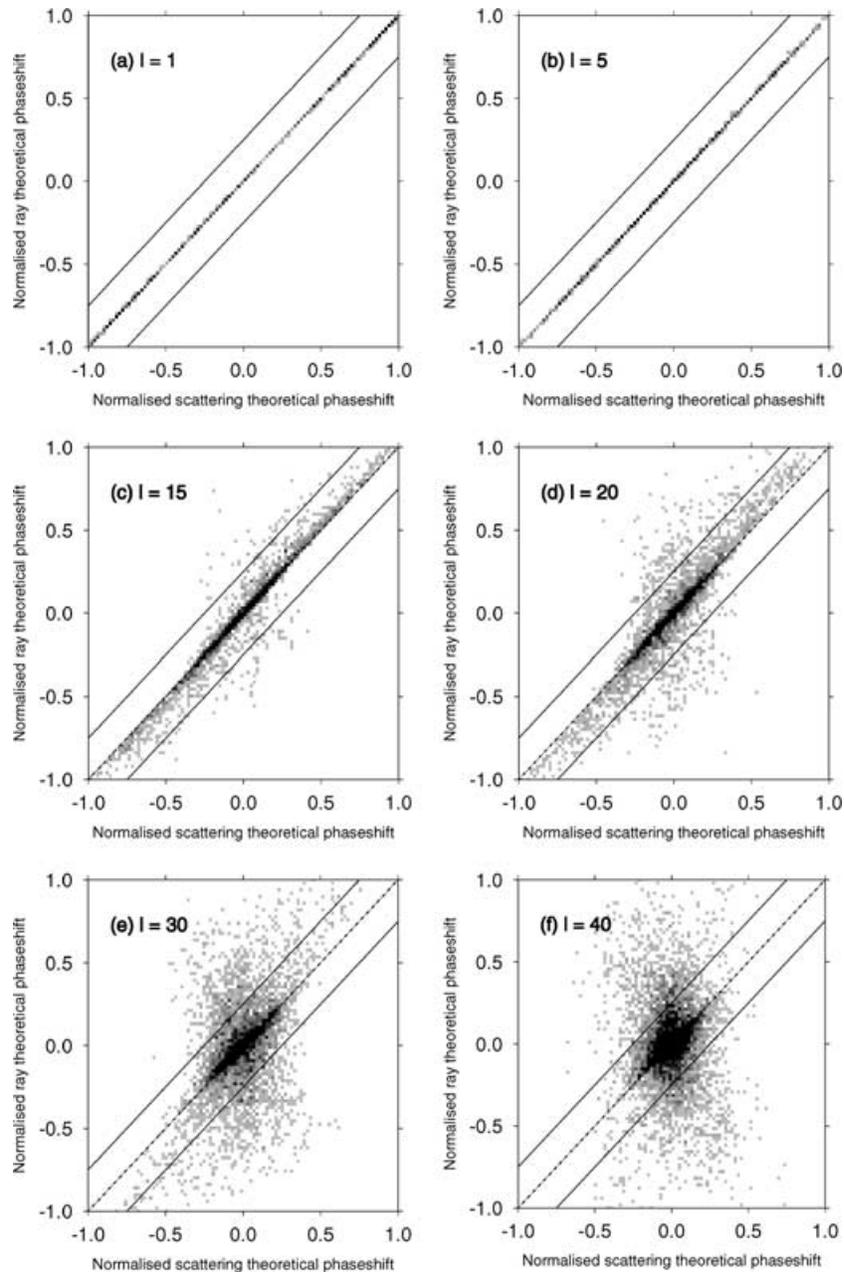
Figure 6. Plots of the scattering theoretical phaseshift versus the ray theoretical phaseshift for spherical harmonic models with the characteristic length of heterogeneity expressed as an angular degree l. The case of Love waves at 150 s is considered, and the source–receiver positions for the computation of the phaseshifts are from Trampert & Woodhouse (2001). The two solid lines indicate the measurement error in the surface wave data set for Love waves at 150 s. (A) $l = 1$, (B) $l = 5$, (C) $l = 15$, (D) $l = 20$, (E) $l = 30$, (F) $l = 40$.

spectrum, the synthetic experiment presented in this paper indicates to what extent the ray theoretical great circle approximation differs from a more exact scattering theory. The relative error owing to the great circle approximation should not exceed the observed relative error in the data. The phase velocity measurements from Trampert & Woodhouse (2001) have a relative error of about 20 per cent for Love waves at 40 s and a relative error of 40 per cent for Love waves at 150 s. Using the results in Fig. 5, we see that ray theoretical surface wave tomography is limited to angular degrees smaller than approximately $l = 25$ and 15 for Love waves at 40 and 150 s, respectively. If we want to retrieve higher angular degrees in our models we should

take the non-ray geometrical effect of surface waves into account. Otherwise, we may obtain inaccurate surface wave Earth models because of an inappropriate usage of ray theory.

In Figs 6(A)–(F), we present plots of the scattering theoretical phaseshift versus the ray theoretical phaseshift for Love waves at 150 s. Fig. 6 is similar to the plots that are found in Baig *et al.* (2000). Again, the source–receiver positions are from the data set of Trampert & Woodhouse (2001). Spherical harmonic input models with the length-scale of inhomogeneity related to the angular degree l are used in Figs 6(A) $l = 1$, (B) $l = 5$, (C) $l = 15$, (D) $l = 20$, (E) $l = 30$ and (F) $l = 40$. We have chosen to plot the normalized

phaseshifts calculated with scattering theory and ray theory. The solid lines indicate the error in the Love waves data set at 150 s. We see in Figs 6(A) and (B) that there is a one-to-one correspondence between the scattering theoretical phaseshifts and the ray theoretical phaseshifts. In Figs 6(C) $l = 15$ and (D) $l = 20$ where the angular degree of inhomogeneity is at the limit of the regime of the great circle approximation for Love waves at 150 s, it is noted that several points of d^{scat} versus d^{ray} are outside the observed error in the data set. It is also apparent in Figs 6(C) and (D) that the points in the plot are slightly rotated anticlockwise compared with the dashed-dotted line with a slope of one through the origin. There is therefore a tendency for there to be a systematic error.

In Figs 6(E) and (F), the picture differs more and more from that in the previous plots of Fig. 6. The points of d^{scat} versus d^{ray} are rotated more and more anticlockwise with increasing angular order. In Fig. 6(F), the best-fitting line (not shown) is such that the positive scattering theoretical phaseshift corresponds to a negative ray theoretical phaseshift and vice versa. Hence the ray theoretical great circle approximation produces global maps with the wrong sign in the small-scale structure. Another such example of the failure of ray theory is found in Fig. 4 of Spetzler & Snieder (2001) where it is clearly shown that ray theory not only produce too large timeshifts compared with the observed ones, but the sign of the predicted residual times owing to ray theory also has the wrong sign. Yet another example of this trend is demonstrated in Spetzler *et al.* (2002) where ray theory and scattering theory are tested in a laboratory experiment and in a numerical finite-difference experiment using heterogeneous small-scale structured media.

It is not difficult to compute the sensitivity kernels discussed here. The developed scattering approach for surface waves is just as easy to use as the ray theoretical great circle approximation. On a 250 MHz Ultrasparc machine, it takes a few days of CPU time to compute the tabulated scattering sensitivity kernels for relative phase velocity measurements or group velocity measurements needed to carry out the inversion of surface wave data for a phase or group velocity map to angular degree and order 40.

In a second stage of inversion, it can be envisaged that we would update the Fréchet kernels in a heterogeneous reference model. This would take bending, focusing and defocusing of the wavefronts into account using essentially the same theory as presented above. Theoretically, this is possible, but is still limited by computational resources.

6 CONCLUSIONS

We have investigated the non-ray geometrical effect in global surface wave tomography. The first-order Rytov approximation was used to derive a linear relationship between surface wave phase and group velocity measurements and relative phase and group velocity perturbations, respectively. The scattering approach takes the finite-frequency effect of surface waves into account, which is not possible with conventional ray theory in surface wave tomography. For finite-frequency surface waves, the sensitivity to the relative phase velocity is maximum in magnitude off the path of the ray trace. The scattering sensitivity kernel for the relative phase velocity at short periods only has sidelobes outside the first Fresnel zone. Given the same strength of heterogeneity, scattering of surface waves becomes increasingly important for increasing period and epicentral distance.

We applied phaseshift measurements for Love waves with periods of between 40 and 150 s from Trampert & Woodhouse (2001)

to compile global phase velocity maps to angular degree and order 40 using scattering theory. These models for diffraction theory were matched with those computed with ray theory. We applied an *a priori* Laplacian smoothness condition in the inversion procedure, resulting in that only structures to angular degree 20–25 for Love waves at 40 s and to angular degree 10–15 for Love waves at 150 s are present in the phase velocity maps, which is close to the limit of resolution in current global surface wave tomography. We saw that ray theory and scattering theory produce the same tomographic models in the regime for which the conditions for ray theory are satisfied.

However, in a synthetic experiment with a velocity inhomogeneity with increasing angular degree, we showed that the scattering of surface waves is dominant at angular degrees greater than $l = 15$ and 25 for surface waves at 150 and 40 s, respectively. The regime of surface wave scattering theory starts at the limits of present-day resolution in surface wave tomography. Consequently, in order to obtain detailed higher-degree surface wave models using long-period surface waves or a data set with many long source–receiver distances we must take the finite-period effect of surface waves into account.

In the USArray project, the United States will be covered with a dense array of 2000 seismographs having a uniform station spacing over the next ten years (see Levander *et al.* 1999). The purpose of the USArray is to increase the resolution of tomographic images of the North American shield. However, it is not enough to increase the data coverage of the area of interest, but it is also important to improve the tomographic imaging methodology that is to be applied in inversions of data from the USArray project.

REFERENCES

Abramowitz, M. & Stegun, I.A., 1970. *Handbook of Mathematical Functions: with Formulas, Graphs and Mathematical Tables,* Dover, New York.

Backus, G.E., 1964. Geographical interpretation of measurements of average phase velocities of surface waves over great circular and great semi circular paths, *Bull. seism. Soc. Am.,* **54,** 571–610.

Baig, A., Dahlen, F.A. & Hung, S.H., 2000. The efficacy of Born kernels for computation of traveltimes in random media, abstract at AGU 2000 Fall meeting, **S62A-01**.

Dahlen, F.A., 1979. The spectra of unresolved split normal mode multiplets, *Geophys. J. R. astr. Soc.,* **58,** 1–33.

Dahlen, F.A. & Tromp, J., 1998. *Theoretical Global Seismology,* Princeton University Press, Princeton, NJ.

Dahlen, A., Hung, S.H. & Nolet, G., 2000. Fréchet kernels for finite-frequency traveltimes—I. Theory, *Geophys. J. Int.,* **141,** 157–174.

Dziewonski, A.M., 1984. Mapping the lower mantle: determination of lateral heterogeneity in *P*-velocity up to degree and order 6, *J. geophys. Res.,* **89,** 5929–5952.

van Heijst, H.J. & Woodhouse, J., 1999. Global high-resolution phase velocity distributions of overtone and fundamental-mode surface waves determined by mode branch stripping, *Geophys. J. Int.,* **137,** 601–620.

Hung, S.H., Dahlen, A. & Nolet, G., 2000. Fréchet kernels for finite-frequency traveltimes—II. Examples, *Geophys. J. Int.,* **141,** 175–203.

Jordan, T.H., 1978. A procedure for estimating lateral variations from low frequency eigenspectra data, *Geophys. J. R. astr. Soc.,* **52,** 441–455.

Kravtsov, Y.A., 1988. Rays and caustics as physical objects, in *Progress in Optics,* Vol. XXVI, pp. 227–348, ed. Wolf, E., Elsevier, Amsterdam.

van der Lee, S. & Nolet, G., 1997. Upper mantle *S*-velocity structure of north America, *J. geophys. Res.,* **102,** 22 815–22 838.

Levander, A., Humphreys, E.G., Ekstrom, G., Meltzer, A.S. & Shearer, P.M., 1999. Proposed project would give unprecedented look under north America, *EOS,* **80,** 250–251.

Marquering, H., Nolet, G. & Dahlen, F.A., 1998. Three-dimensional waveform sensitivity kernels, *Geophys. J. Int.,* **132,** 521–534.

Marquering, H., Dahlen, F.A. & Nolet, G., 1999. The body-wave travel-time paradox: bananas, doughnuts and 3-D delay-time kernels, *Geophys. J. Int.,* **137,** 805–815.

Menke, W., 1989. *Geophysical Data Analysis: Discrete Inverse Theory,* Academic Press, New York.

Menke, W. & Abbot, D., 1990. *Geophysical Theory,* Columbia University Press, NY.

Passier, M.L. & Snieder, R., 1995. Using differential waveform data to retrieve local *S*-velocity structure or path-averaged *S*-velocity gradients, *J. geophys. Res.,* **100,** 24 061–24 078.

Snieder, R., 1986. The Influence of topography on the propagation and scattering of surface waves, *Phys. Earth planet. Inter.,* **44,** 226–241.

Snieder, R., 1988. Large-scale waveform inversions of surface waves for lateral heterogeneity 1. Theory and numerical examples, *J. geophys. Res.,* **93,** 12 055–12 065.

Snieder, R., 1993. Global inversions using normal mode and long-period surface waves, in *Seismic Tomography: Theory and Practice,* pp. 23–63, Chapman and Hall, London, UK.

Snieder, R. & Lomax, A., 1996. Wavefield smoothing and the effect of rough velocity perturbations on arrival times and amplitudes, *Geophys. J. Int.,* **125,** 796–812.

Snieder, R. & Nolet, G., 1987. Linearized scattering of surface waves on a spherical earth, *J. geophys. Res.,* **61,** 55–63.

Snieder, R. & Romanowicz, B., 1988. A new formalism for the lateral heterogeneity on normal modes and surface waves—I: Isotropic perturbations, perturbations of interfaces and gravitational perturbations, *Geophys. J. R. astr. Soc.,* **92,** 207–222.

Spetzler, J. & Snieder, R., 2001. The effects of small-scale heterogeneity on the arrival time of waves, *Geophys. J. Int.,* **145,** 786–796.

Spetzler, J., Sivaji, C., Nishizawa, O. & Fukushima, Y., 2002. A test of ray theory and scattering theory based on a laboratory experiment using ultrasonic waves and numerical simulations by finite-difference method, *Geophys. J. Int.,* **148,** 165–179.

Spetzler, J., Trampert, J. & Snieder, R., 2001. Are we exceeding the limits of the great circle approximation in global surface wave tomography?, *Geophys. Res. Lett.,* **28,** 2341–2344.

Tong, J., Dahlen, F.A., Nolet, G. & Marquering, H., 1998. Diffraction effects upon finite-frequency travel times: a simple 2-D example, *Geophys. Res. Lett.,* **25,** 1983–1986.

Trampert, J. & Woodhouse, J.H., 1995. Global phase velocity maps of Love and Rayleigh waves between 40 and 150 seconds, *Geophys. J. Int.,* **122,** 675–690.

Trampert, J. & Woodhouse, J.H., 2001. Assessment of global phase velocity models, *Geophys. J. Int.,* **144,** 165–174.

Yomogida, K., 1992. Fresnel zone inversion for lateral heterogeneities in the earth, *Pure appl. Geophys.,* **138,** 391–406.

Yomogida, K. & Aki, K., 1987. Amplitude and phase data inversion for phase velocity anomalies in the Pacific ocean basin, *Geophys. J. R. astr. Soc.,* **88,** 161–204.

Woodward, M.J., 1992. Wave-equation tomography, *Geophysics,* **57,** 15–26.

Woodhouse, J.H. & Dziewonski, A.M., 1984. Mapping the upper mantle: three-dimensional modeling of earth structure by inversion of seismic wavefroms, *J. geophys. Res.,* **89,** 5953–5986.

Woodhouse, J.H. & Girnuis, T.P., 1982. Surface waves and free oscillations in a regional earth model, *Geophys. J. R. astr. Soc.,* **68,** 653–673.

Zhao, L., Jordan, T.H. & Chapman, C.H., 2000. Three-dimensional Fréchet differential kernels for seismic delay times, *Geophys. J. Int.,* **141,** 558–576.

APPENDIX A: PERTURBATION THEORY OF THE PROPAGATION LENGTH OF SCATTERED RAY PATHS, THE WIDTH OF THE FRESNEL ZONE AND THE GEOMETRICAL FACTOR

According to Fig. A1 the epicentral distance between the source and receiver is denoted by Δ_{off}, and the epicentral distance between the source and scatterer point and the scatterer point and receiver are marked as Δ_1 and Δ_2, respectively. The perpendicular distance from the source–receiver geometry to the scatterer at the offset φ is $|\theta - \pi/2|$. Using the law of cosines on a sphere to relate Δ_1 with $|\theta - \pi/2|$ and φ, we obtain

$$\cos(\Delta_1) = \cos\left(\left|\theta - \frac{\pi}{2}\right|\right)\cos(\varphi) + \sin\left(\left|\theta - \frac{\pi}{2}\right|\right)$$
$$\times \sin(\varphi)\cos\left(\frac{\pi}{2}\right) = \cos\left(\left|\theta - \frac{\pi}{2}\right|\right)\cos(\varphi). \quad (A1)$$

Isolating Δ_1 from eq. (A1) and assuming that the ray deflection $|\theta - \pi/2|$ is small gives

$$\Delta_1 = \arccos\left[\cos\left(\left|\theta - \frac{\pi}{2}\right|\right)\cos(\varphi)\right]$$
$$\approx \arccos\left[\cos(\varphi) - \frac{1}{2}\left(\theta - \frac{\pi}{2}\right)^2\cos(\varphi)\right]$$
$$\approx \varphi + \frac{\left(\theta - \frac{\pi}{2}\right)^2}{2\tan(\varphi)}. \quad (A2)$$
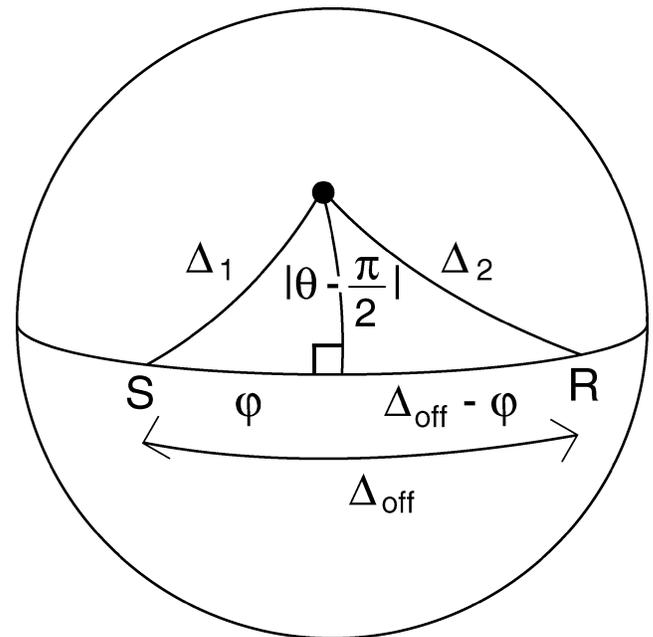
Figure A1. Explanation of the variables applied in the derivation of the propagation length of a scattered ray path, the width of the Fresnel zone on the sphere and the geometrical factor using second-order perturbation theory.

Similarly, we have for Δ_2 that

$$\Delta_2 = (\Delta_{\text{off}} - \varphi) + \frac{\left(\theta - \frac{\pi}{2}\right)^2}{2 \tan(\Delta_{\text{off}} - \varphi)}. \tag{A3}$$

The detour (i.e. $\Delta_1 + \Delta_2 - \Delta_{\text{off}}$) is then given by

$$\Delta_1 + \Delta_2 - \Delta_{\text{off}} = \frac{\left(\theta - \frac{\pi}{2}\right)^2}{2} \left[\frac{1}{\tan(\varphi)} + \frac{1}{\tan(\Delta_{\text{off}} - \varphi)} \right]$$

$$= \frac{\left(\theta - \frac{\pi}{2}\right)^2}{2} \frac{\sin(\Delta_{\text{off}})}{\sin(\varphi)\sin(\Delta_{\text{off}} - \varphi)}. \tag{A4}$$

The condition for Fresnel zones on a sphere that the detour is less than the wavelength divided by a number n is given by

$$\Delta_1 + \Delta_2 - \Delta_{\text{off}} \leq \frac{\lambda}{n}, \tag{A5}$$

where λ is the wavelength measured in radians. The equality sign in eq. (A5) is used to calculate the Fresnel zone boundary. By inserting the detour in eq. (A4) in the Fresnel zone condition in eq. (A5), the half-width $(\theta - \frac{\pi}{2})$ of Fresnel zones is derived, hence

$$\left(\theta - \frac{\pi}{2}\right) = \sqrt{\frac{2\lambda \sin(\varphi)\sin(\Delta_{\text{off}} - \varphi)}{n \sin(\Delta_{\text{off}})}}, \tag{A6}$$

which has the largest value for $\varphi = \Delta_{\text{off}}/2$. For that case, the half-width of the Fresnel zone is given by

$$\left(\theta - \frac{\pi}{2}\right) = \sqrt{\frac{\lambda}{n} \tan\left(\frac{\Delta_{\text{off}}}{2}\right)}. \tag{A7}$$

The maximum width L_F of Fresnel zones on the sphere is twice the half-width $(\theta - \frac{\pi}{2})$ in eq. (A7), thus

$$L_F = \sqrt{\frac{4\lambda}{n} \tan\left(\frac{\Delta_{\text{off}}}{2}\right)}, \tag{A8}$$

where L_F and λ are measured in radians.

The geometrical factors $\sin(\Delta_1)$ and $\sin(\Delta_2)$ are derived to a zeroth-order approximation using eqs (A2) and (A3), thus

$$\sin(\Delta_1) = \sin(\varphi) \quad \text{and} \quad \sin(\Delta_2) = \sin(\Delta_{\text{off}} - \varphi), \tag{A9}$$

where it is assumed that $(\theta - \pi/2)^2/[2\tan(\varphi)] \ll 1$ and $(\theta - \pi/2)^2/[2\tan(\Delta_{\text{off}} - \varphi)] \ll 1$.

APPENDIX B: THE SCATTERING SENSITIVITY KERNEL FOR MAJOR ARCS

The scattering sensitivity kernel to compute phase velocity maps for major arcs (e.g. $\pi < \Delta_{\text{off}} < 2\pi$) can be constructed by three scattering sensitivity kernels for minor arcs. Let the scattering sensitivity kernels for the minor arcs between the source (S) and the receiver antipod (RA), between the receiver antipod and the source antipod (SA) and between the source antipod and receiver (R) be given by

$$K_{l,m}^{\text{scat,ph},S\to RA}(\Delta_{\text{off}} - \pi, \nu_0) = \int_0^{\Delta_{\text{off}} - \pi} \int_0^{\pi} Y_l^m(\theta, \varphi)$$
$$\times K^{\text{ph},S\to RA}(R, \theta, \varphi)\,d\theta\,d\varphi, \tag{B1}$$

$$K_{l,m}^{\text{scat,ph},RA\to SA}(2\pi - \Delta_{\text{off}}, \nu_0) = \int_{\Delta_{\text{off}} - \pi}^{\pi} \int_0^{\pi} Y_l^m(\theta, \varphi)$$
$$\times K^{\text{ph},RA\to SA}(R, \theta, \varphi)\,d\theta\,d\varphi, \tag{B2}$$

and

$$K_{l,m}^{\text{scat,ph},SA\to R}(\Delta_{\text{off}} - \pi, \nu_0) = \int_{\pi}^{\Delta_{\text{off}}} \int_0^{\pi} Y_l^m(\theta, \varphi)$$
$$\times K^{\text{ph},SA\to R}(R, \theta, \varphi)\,d\theta\,d\varphi, \tag{B3}$$

where the sensitivity kernels $K^{\text{ph},S\to RA}(R, \theta, \varphi)$, $K^{\text{ph},RA\to SA}(R, \theta, \varphi)$ and $K^{\text{ph},SA\to R}(R, \theta, \varphi)$ are equivalent to the sensitivity kernel in eq. (16) but having the epicentral distance substituted with $\Delta_{\text{off}} - \pi$, $2\pi - \Delta_{\text{off}}$ and $\Delta_{\text{off}} - \pi$, respectively. In order to derive the sensitivity kernel $K_{l,m}^{\text{scat,ph}}(\Delta_{\text{off}}, \nu_0)$ owing to scattering theory for major arcs, the integration along the source–receiver line is split up into the three minor arc integrations. Hence,

$$K_{l,m}^{\text{scat,ph}}(\Delta_{\text{off}}, \nu_0) = \frac{1}{\Delta_{\text{off}}} \left[(\Delta_{\text{off}} - \pi)K_{l,m}^{\text{scat,ph},S\to RA}(\Delta_{\text{off}} - \pi, \nu_0) \right.$$
$$+ (2\pi - \Delta_{\text{off}})K_{l,m}^{\text{scat,ph},RA\to SA}(2\pi - \Delta_{\text{off}}, \nu_0)$$
$$\left. + (\Delta_{\text{off}} - \pi)K_{l,m}^{\text{scat,ph},SA\to R}(\Delta_{\text{off}} - \pi, \nu_0) \right], \tag{B4}$$

which is the formula in eq. (26). Similarly, by dividing the major arc into three minor arcs, the formula in eq. (27) for the scattering sensitivity kernel for group velocity measurements can be derived.

APPENDIX C: ROTATION OF SCATTERING SENSITIVITY KERNELS

Dziewonski (1984) and Dahlen & Thromp (1998) show that the transformation of the spherical harmonics of angular degree l and order m from a reference coordinate system to a new coordinate system is given by

$$Y_l^m(\theta, \varphi) = \exp(im\Phi) \sum_{n=-l}^{l} \exp(in\Psi)Q_l^{m,n}(\Theta)Y_l^n(\theta', \varphi'), \tag{C1}$$

with the three Euler angles denoted by Φ, Ψ and Θ, and the elements of the rotation matrix are $Q_l^{m,n}(\Theta)$. The sensitivity kernel for minor arcs in eq. (18) depends linearly on the spherical harmonics. This means that the sensitivity kernel for the relative phase velocity using scattering theory can be transformed from the reference coordinate system into the observed coordinate system using the relation for the transformation of spherical harmonics in eq. (C1). Let $K^{\text{ph}*}(R, \theta, \varphi)$ denote the sensitivity kernel in the observed coordinate system, which is equivalent to the sensitivity kernel $K^{\text{ph}}(R, \theta, \varphi)$ in eq. (16) in the reference coordinate system. The formula in eq. (C1) is inserted in the scattering sensitivity kernel in eq. (18). The sensitivity kernel $K_{l,m}^{\text{scat,ph}}(\Delta_{\text{off}}, \nu_0)$ for the epicentral offset Δ_{off} in the new coordinate system is then

$$K_{l,m}^{\text{scat,ph}}(\Delta_{\text{off}}, \nu_0) = \iint_{\mathbf{r}_S}^{\mathbf{r}_R} Y_l^m(\theta, \varphi)K^*(R, \theta, \varphi)\,d\theta\,d\varphi$$

$$= \exp(im\Phi) \sum_{n=-l}^{l} \exp(in\Psi)Q_l^{m,n}(\Theta)$$

$$\times \int_0^{\Delta_{\text{off}}} \int_0^{\pi} Y_l^n(\theta', \varphi')K(R, \theta', \varphi')\,d\theta'\varphi'$$

$$= \exp(im\Phi) \sum_{n=-l}^{l} \exp(in\Psi)Q_l^{m,n}(\Theta)$$

$$\times K_{l,n}^{\text{scat,ph}}(\Delta_{\text{off}}, \nu_0), \tag{C2}$$

with the scattering sensitivity kernel for relative phase velocity being given by

$$K_{l,n}^{\text{scat,ph}}(\Delta_{\text{off}}, \nu_0) = \int_0^{\Delta_{\text{off}}} \int_0^{\pi} Y_l^n(\theta', \varphi') K^{\text{ph}}(R, \theta', \varphi')\, d\theta'\, d\varphi',$$

(C3)

at an offset of Δ_{off} computed in the reference coordinate system.

The scattering sensitivity kernels in eqs (26) and (27) for major arcs are composed of three scattering sensitivity kernels for minor arcs. It is therefore possible to apply the transformation of spherical harmonics in eq. (C1) on each scattering sensitivity kernel for minor arcs in order to obtain the same result as in eq. (C2), but with the scattering kernel for major arcs computed in the reference coordinate system. In addition, the result in eq. (C2) is valid for major arc sensitivity kernels using scattering theory to compute group velocity maps.